

# Minimizing EIT image artefacts from mesh variability in Finite Element Models

Andy Adler<sup>1</sup>, William R B Lionheart<sup>2</sup>

<sup>1</sup>Systems and Computer Engineering, Carleton University, Ottawa, Canada

<sup>2</sup>School of Mathematics, University of Manchester, UK

**Abstract.** Electrical Impedance Tomography solves an inverse problem to estimate the conductivity distribution within a body from electrical simulation and measurements at the body surface, where the inverse problem is based on a solution of Laplace's equation in the body. Most commonly, a finite element model (FEM) is used, largely because of its ability to describe irregular body shapes. In this paper, we show that simulated variations in the positions of internal nodes within a FEM can result in serious image artefacts in the reconstructed images. Such variations occur when designing FEM meshes to conform to conductivity targets, but the effects may also be seen in other applications of absolute and difference EIT. We explore the hypothesis that these artefacts result from changes in the projection of the anisotropic conductivity tensor onto the FEM system matrix, which introduces anisotropic components into the simulated voltages, which cannot be reconstructed onto an isotropic image, and appear as artefacts. The magnitude of the anisotropic effect is analyzed for a small regular FEM, and shown to be proportional to the relative node movement as a fraction of element size. In order to address this problem, we show that it is possible to incorporate a FEM node movement component into the formulation of the inverse problem. These results suggest that it is important to consider artefacts due to FEM mesh geometry in EIT image reconstruction.

*Keywords:* Electrical Impedance Tomography, Image Reconstruction, Finite Element Models, EIT Simulation Anisotropy

## 1. Introduction

This paper describes the image reconstruction artefacts which occur in electrical impedance tomography (EIT) images due to limitations in finite element models. We develop a hypothesis to explain these artefacts, show results to support it, and then develop an image reconstruction method to reduce these artefacts. EIT is a technology designed to measure conductivity changes within a body using electrical stimulations and measurements at electrodes on the body surface. Typically, patterns of alternating currents are sequentially applied to the electrodes and the resulting voltages measured. This set of measurements constitutes an EIT data frame, from which images may then be reconstructed of the body's internal impedance distribution (absolute imaging) or the change in impedance distribution between two data frames (difference imaging).

EIT thus has the advantage of providing tomographic information about a body from measurements using equipment which is non-invasive, minimally cumbersome and potentially inexpensive (Holder, 2005).

Reconstruction of EIT images requires solving an ill-posed inverse problem. EIT has low sensitivity to interior contrasts due to the physics of current propagation; most current stays close to the source electrodes on the body surface, while only a much smaller fraction penetrates the interior, which is typically the region of interest. One further consequence of the current propagation is the extreme sensitivity to the shape of the body surface and exact electrode placements and properties (Soleimani *et al* 2005). One technique to deal with shape and electrode uncertainties is the use of time difference imaging, in which is less sensitive to shape uncertainties which do not change between data frames (eg. Adler *et al* 1996b).

The earliest approaches to EIT image reconstruction were based on 2D circular approximations of the thorax (Seagar and Bates, 1985; Barber and Brown, 1988). However, since such analytical models cannot describe electrical propagation in complex, realistic body shapes, finite element models (FEM) have been used (Murai and Kagawa, 1985; Yorkey *et al* 1987). Over the last two decades, the FEM has become the most popular approach to model EIT physics. Other numerical models, such as those based on finite differences (Yang and Patterson, 2007) have been used; however, the FEM continues to be popular because finite element mesh elements can conform to arbitrary body shapes and be refined in regions of high electric field, such as near to electrodes. Most EIT research has used the simplest FEM structure using simplex elements (triangles in 2D and tetrahedrons in 3D) and conductivity modelled as piecewise constant (so that changes in conductivity occur only at element boundaries). Such choices are reasonable: all FEM meshing packages provide good support for simplex elements, and anatomically realistic conductivity changes do occur abruptly at organ boundaries. Additionally, two further FEM approximations are typically made: 1) first order elements are used, which interpolate voltage across each element linearly between nodes. Physically, such elements may be modelled by a resistor network (Murai and Kagawa, 1985). Such a FEM is easier to conceptualize and may be used as the basis for a physical resistor network model of the medium (Gagnon *et al* 2010). On the other hand, FEM errors decrease linearly with element size for first order FEMs, while the rate of error decrease is larger for higher order models (Silvester and Ferrari 1990). 2) the conductivity is assumed to be isotropic. While many tissues are (macroscopically) anisotropic, it is difficult to measure these properties and few published values exist. Thus, it has been common to simply ignore anisotropy in an EIT model. On the other hand, the anisotropic effects can be included into the FEM fairly straightforwardly (Abascal *et al* 2008).

The most common approach to image reconstruction in EIT has been to parametrize the conductivity distribution vector,  $\mathbf{m}$ , as piecewise constant over each FEM element. The reconstructed conductivity (or conductivity change) distribution,  $\hat{\mathbf{m}}$  is then

calculated from data (or difference data),  $\mathbf{d}$  as

$$\hat{\mathbf{m}} = \arg \min_{\mathbf{m}} \|\mathbf{d} - F(\mathbf{m})\|_{\Sigma_n}^2 + \|\mathbf{m} - \mathbf{m}_0\|_{\Sigma_d}^2 \quad (1)$$

where  $F(\mathbf{m})$  represents the FEM voltages (absolute imaging) or voltage differences (difference imaging),  $\Sigma_n$  the covariance of electronic measurement noise, and  $\bar{\mathbf{m}}$  and  $\Sigma_m$ , respectively, are the image prior expected mean and covariance. In this way, the reconstructed image,  $\hat{\mathbf{m}}$ , is the selection of FEM conductivity parameters which best fits the data and prior model.

In this paper, we report that this approach to image reconstruction is very sensitive to any geometrical variability in the FEM. For example, a small change in the positions of internal nodes, even if it preserves the conductivity distribution, can result in large image reconstruction artefacts. This effect was unexpected, since the voltage distribution simulated by the FEM is accurate even for moderately dense models. This paper expands on our previous report (Adler *et al* 2008), and we are not aware of previous reports of this phenomenon. This effect may explain a few puzzling results. For example, studies of electrode movement have often used FEM simulations to show that unacceptable artefacts occur for very small electrode displacements (Breckon and Pidcock 1988, Adler *et al* 1996b). On the other hand, experimentally, electrode movements which are an order of magnitude greater, such as the movement of  $> 1$  cm for thoracic imaging, still permit usable images.

In the following sections, we first illustrate the effect for 2D and 3D FEMs. Next, we show how this effect is related to anisotropic conductivity contributions, and analyse the magnitude of the effect as a function of FEM geometry. We then develop a hypothesis which may explain the effect, and show numerical and model evidence to support it. Finally we propose an approach to modify image reconstruction which dramatically reduces these image artefacts.

## 2. Geometry variability example

FEM accuracy is normally considered from the point of view of voltage errors between the FEM and physical phantom. In this case, any errors may be explained by small details in the phantom which are not considered in the model, which means that it is difficult to use such a test to verify high model accuracy. Here, we evaluate a FEM model by looking at small changes in the model and the consequences on difference EIT images. In difference EIT, the difference image,  $\mathbf{m} = \boldsymbol{\sigma} - \boldsymbol{\sigma}_r$ , between conductivity distribution,  $\boldsymbol{\sigma}$ , and a reference distribution,  $\boldsymbol{\sigma}_r$ , is calculated from difference measurements,  $\mathbf{d} = \mathbf{v} - \mathbf{v}_r$ , where  $\mathbf{v}$  and  $\mathbf{v}_r$  represent the current and reference frames of EIT data. In this section, we show how re-meshing around a circular object can introduce large artefacts into the reconstructed difference images.

We study difference imaging and a linear reconstruction in order to represent the artefacts or errors. Iterative calculations, such as those needed for absolute imaging, will accumulate such errors at each iteration stage. The easiest (and most common) way to

simulate a target in a medium is to use a single FEM to select and then interpolate the elements which are part of the target. There are then no changes to the underlying FEM, and thus no model difference artefacts in the images. A more accurate representation of a target is to create a target region within the FEM and to re-mesh around it. In this case, the mesh will change between each target position, not only near the target, but throughout the FEM due to the propagation of changes in triangularization.

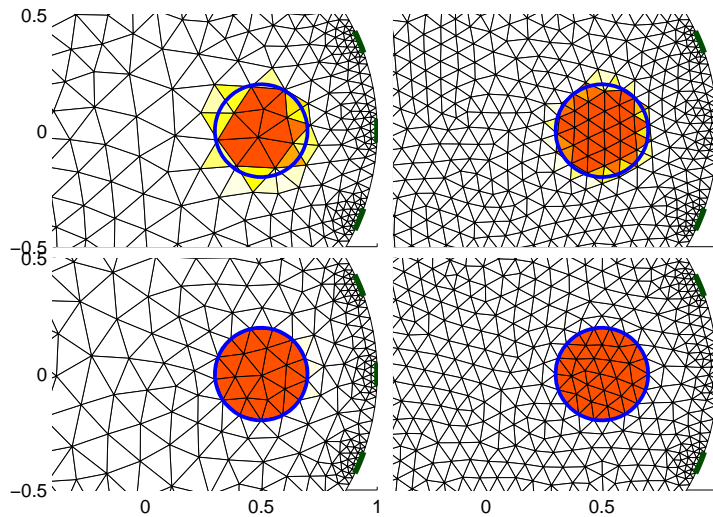


**Figure 1.** Simulation FEMs and simulated conductivity target positions (within blue circle). Electrode nodes are indicated in green. An inner region surrounding a target is shown. *Left:* Coarse meshes (maximum mesh size of 0.16, 1441 triangles) *Right:* Fine meshes (maximum mesh size of 0.07, 1941 triangles) *Top:* Meshes with no adaptation for target. Element conductivity is defined by region membership. *Bottom:* Meshes adapted to target region.

To illustrate this process, figure 1 shows 2D circular FEMs with 16 electrodes with local refinement of the FEM near each electrode. Meshes were generated using Netgen (Schöberl, 1997) by defining constructive solid geometry shapes for the medium, electrodes and inclusion. Coarse and fine meshes are calculated by controlling the maximum permissible element size. Two different strategies to specify the region of a simulated conductivity target region are shown. On top, the mesh is not adapted to the target. The conductivity of each element is selected based on the membership in the target region (an element with 50% of its area in the region will have a target conductivity of the average of the background and target region). On the bottom, the FEM is adapted to the target region, resulting in mesh geometry changes which propagate throughout the FEM.

For these models, EIT data were simulated using a Sheffield-type adjacent stimulation and measurement protocol, and images are reconstructed on a coarse 2D regular mesh geometry (shown in figure 2). A one-step Gauss Newton reconstruction is used with a scaled diagonal image prior (Cheney *et al* 1990), and the regularization parameter is chosen such that the noise figure is 1.0 (Adler and Guardo 1996a). Images in

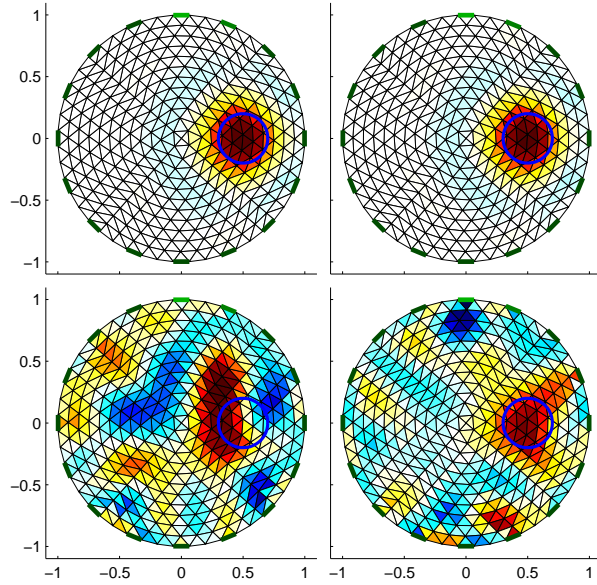


**Figure 2.** Reconstructed difference images calculated from the simulation FEMs (figure 1) on a 576 element 2D mesh. *left* Coarse meshes, and *right* Fine meshes. *Top* Difference images with both data frames simulated on the same geometry, and interpolated target conductivities. *Bottom* Difference images with targets simulated of different mesh geometries:  $\mathbf{v}_r$  on *top* FEM, and  $\mathbf{v}$  on *bottom* FEM (adapted to target). The simulation target position is indicated by the blue circle.

which the simulation mesh geometry matched exactly (figure 2, *top*) show the expected location and shape. However, when the mesh geometry changes between difference data simulations (figure 2, *bottom*) artefacts occur throughout the images. Reconstruction artefacts decrease as the FEM density increases, due to the increase in accuracy of the FEM with decreasing mesh size.

Similar artefacts occur for 3D simulations; however, the effect is considerably larger because many more FEM elements are required to achieve the same level of refinement (mesh size reduction) in 3D compared to 2D. In figure 3, 3D FEMs are created corresponding to the 2D simulations in figure 1, with a cylinder created by vertically extruding the 2D shape (and target position), using circular electrodes at half the cylinder height. In order to show a similar effect, the level of refinement of the coarse and fine mesh were manually adjusted until image artefacts of approximately the same level figure 2 were obtained. Reconstructed images are shown in figure 6 (*right, top*), above the improved images which can be obtained by the algorithm developed in section 4.

In order to quantify the level of image artefact, we calculate reconstructed images for a series of FEM models of increasingly refined mesh size for the 2D and 3D FEM. Difference images are calculated from the pair of simulated measurements from the FEMs with and without adaptation to the target shape. Both models are assigned a homogeneous conductivity, which, except for the effects considered in this paper, should yield a difference image of zero. The resulting image is considered the artefact due to the model, and an image artefact amplitude (AAM) is defined as  $AAM = \sum_i A_i \hat{\mathbf{m}}_i$ ,

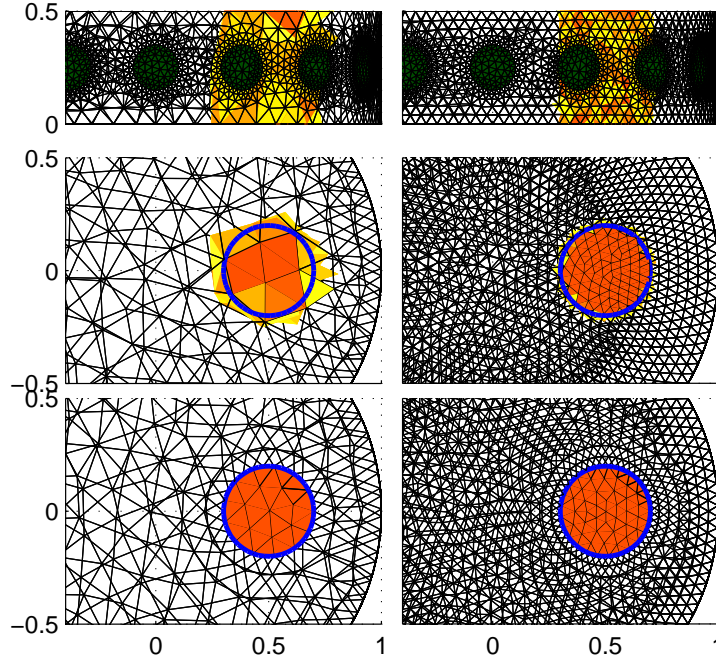


**Figure 3.** Simulation 3D FEMs with a simulated conductivity as a vertical cylinder, with positions (within blue circle). Electrode nodes are indicated in green. *Left:* Coarse meshes (maximum mesh size of 0.18, 5941 triangles) *Right:* Fine meshes (maximum mesh size of 0.05, 19379 triangles) *Top:* Meshes with no adaptation for target, vertical view. *Middle:* Meshes with no adaptation for target. *Bottom:* Meshes adapted to target region.

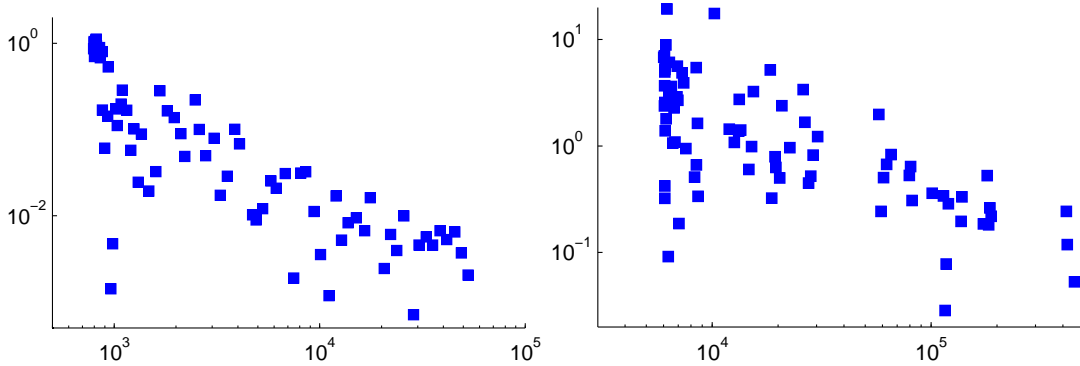


**Figure 4.** Artefact amplitude (normalized to image amplitude from a contrast) in a reconstructed image of the central slice as a function of number of FEM nodes in the simulation model, for: *Left:* 2D simulation models, and *Right:* 3D simulation models.

where  $A_i$  and  $\hat{\mathbf{m}}_i$  represent the area and reconstructed amplitude in FEM element  $i$ ; AAM values are normalized to the image amplitude of the conductive target. Figure 4 shows AAM as a function of the number of nodes in the simulation. AAM decreases with number of FEM nodes, and is larger for 3D models.



and, as a function of the element system matrices ( $\mathbf{S}^{(k)}$ ), the symmetric  $\mathbf{S}$  is

$$\mathbf{S} = \begin{bmatrix} \mathbf{S}_{11}^{(1)} + \mathbf{S}_{11}^{(4)} & \mathbf{S}_{12}^{(1)} & 0 & \mathbf{S}_{12}^{(4)} & \mathbf{S}_{13}^{(1)} + \mathbf{S}_{13}^{(4)} \\ & \mathbf{S}_{22}^{(1)} + \mathbf{S}_{22}^{(2)} & \mathbf{S}_{12}^{(2)} & 0 & \mathbf{S}_{23}^{(1)} + \mathbf{S}_{23}^{(2)} \\ & & \mathbf{S}_{11}^{(2)} + \mathbf{S}_{11}^{(3)} & \mathbf{S}_{12}^{(3)} & \mathbf{S}_{13}^{(2)} + \mathbf{S}_{13}^{(3)} \\ & & & \mathbf{S}_{22}^{(3)} + \mathbf{S}_{22}^{(4)} & \mathbf{S}_{23}^{(3)} + \mathbf{S}_{23}^{(4)} \\ & & & & \mathbf{S}_{33}^{(1)} + \mathbf{S}_{33}^{(2)} + \mathbf{S}_{33}^{(3)} + \mathbf{S}_{33}^{(4)} \end{bmatrix} \quad (3)$$

For element  $k$  of conductivity  $\sigma_k$ , the element system matrix  $\mathbf{S}^{(k)}$  is

$$\mathbf{S}^{(k)} = \frac{1}{D! |\det \mathbf{A}|} \sigma_k \mathbf{B}^T \mathbf{B} \quad (4)$$

where  $\mathbf{A}$  is based on node locations (in 2D, pairs  $r_x^{(k)}, r_y^{(k)}$ ) and where  $\mathbf{B} \in \mathbb{R}^{D \times (D+1)}$  is  $\mathbf{A}$  with the first row removed. For the given FEM, for element #1,

$$\mathbf{A} = \begin{bmatrix} 1 & r_x^{(1)} & r_y^{(1)} \\ 1 & r_x^{(2)} & r_y^{(2)} \\ 1 & r_x^{(3)} & r_y^{(3)} \end{bmatrix}^{-1} = \begin{bmatrix} 1 & s & 0 \\ 1 & 0 & s \\ 1 & d & 0 \end{bmatrix}^{-1} = (\det \mathbf{A})^{-1} \begin{bmatrix} -ds & 0 & s^2 \\ s & 0 & -s \\ d & s-d & -s \end{bmatrix} \quad (5)$$

where  $\det \mathbf{A} = (s^2 - ds)^{-1}$ . Since the other elements are reflections,  $\mathbf{A}$  may be multiplied by a unitary reflection matrix  $\mathbf{R}$  such that  $\mathbf{A}^{(k)} = \mathbf{R}^{(k)T} \mathbf{A}^{(1)} \mathbf{R}^{(k)}$ . Based on these values, and considering  $(\det \mathbf{A})$  is positive for  $s > d$ ,

$$\mathbf{S}^{(k)} = \frac{\sigma_k}{2s(s-d)} \begin{bmatrix} s^2 + d^2 & d(s-d) & -s(s+d) \\ d(s-d) & (s-d)^2 & -s(s-d) \\ -s(s+d) & -s(s-d) & 2s^2 \end{bmatrix}^{-1} \quad (6)$$

where, due to the reflections,  $d$  is replaced by  $-d$  for elements 2 and 3.

We may now calculate the impedance for vertical and horizontal current flow. For a FEM of uniform conductivity  $\sigma$ , the vertical current is calculated setting nodes 1,3 to  $V = 0$  and current  $Q_2 = +1$ ,  $Q_4 = -1$  applied, as shown in figure 5, which yields

$$\begin{bmatrix} Q_2 \\ Q_4 \end{bmatrix} = \begin{bmatrix} \mathbf{S}_{22}^{(1)} + \mathbf{S}_{22}^{(2)} & 0 \\ 0 & \mathbf{S}_{22}^{(3)} + \mathbf{S}_{22}^{(4)} \end{bmatrix} \begin{bmatrix} V_2 \\ V_4 \end{bmatrix} = \sigma \begin{bmatrix} V_2 \\ V_4 \end{bmatrix} \quad (7)$$

From this expression, the impedance  $Z_i$  for current through node  $i$  is calculated, as  $Z_i = V_i/Q_i$ , which gives:  $Z_2 = Z_4 = \sigma^{-1}$ . Here  $\mathbf{S}_{22}^{(1)} + \mathbf{S}_{22}^{(2)} = \mathbf{S}_{22}^{(3)} + \mathbf{S}_{22}^{(4)} = \sigma \left( \frac{(s-d)^2}{2s(s-d)} + \frac{(s+d)^2}{2s(s+d)} \right) = \sigma$ , since the direction of  $d$  is reversed between reflected element pairs (1,2) and (3,4). On the other hand, the horizontal current is calculated setting nodes 2,4 to  $V = 0$  and current  $Q_1 = +1$ ,  $Q_3 = -1$  applied, giving

$$\begin{bmatrix} Q_1 \\ Q_3 \end{bmatrix} = \begin{bmatrix} \mathbf{S}_{11}^{(1)} + \mathbf{S}_{11}^{(4)} & 0 \\ 0 & \mathbf{S}_{11}^{(2)} + \mathbf{S}_{11}^{(3)} \end{bmatrix} \begin{bmatrix} V_1 \\ V_3 \end{bmatrix} = \sigma \begin{bmatrix} \frac{s^2+d^2}{s(s-d)} & 0 \\ 0 & \frac{s^2+d^2}{s(s+d)} \end{bmatrix} \begin{bmatrix} V_1 \\ V_3 \end{bmatrix} \quad (8)$$

From this expression,  $Z_1 = \frac{1-f}{1+f^2} \sigma^{-1}$ , and  $Z_3 = \frac{1+f}{1+f^2} \sigma^{-1}$ , where  $f = d/s$  represents the relative geometric distortion.

This result illustrates the anisotropy; for this simple model, vertical impedance is not affected by the internal deformation, while horizontal impedance is affected by an

amount related to the relative deformation  $f$ . Since the anisotropy is proportional to the relative and not the absolute deformation distance, the anisotropic contribution will continue to be relevant for all FEM sizes.

#### 4. Image Reconstruction Formulation

In this section, we propose an image reconstruction formulation to mitigate this problem. The fact that some errors exist is not surprising – the FEM is, after all, only an approximation. The concern is the size of the image errors; surprisingly large image errors continue to exist (especially in 3D models) even for fine mesh geometries.

We hypothesize that the main source of image reconstruction artefacts is that the simulated EIT measurements cannot be explained by a purely isotropic conductivity on a fixed mesh. A selection of a particular FEM geometry is equivalent to a particular representation of the (potentially anisotropic) conductivity tensors on each tetrahedron onto the FEM system matrix. A first-order FE model is equivalent to a resistor on each FE mesh edge, so the maximum degrees of freedom in the FEM is the number of edges. Since there are more edges than elements (by a factor of approx  $\frac{3}{2}$  in 2D and 2 in 3D), not all FEM matrices correspond to isotropic conductivities, and any distortion of the mesh will (typically) be consistent only with an anisotropic conductivity on the original mesh (Abascal *et al* 2011). Difficulties associated with recovering anisotropic conductivities using a FEM model on geophysical data were explored by Herwanger *et al* (2004). Any change in the FEM geometry projects this conductivity tensor differently, resulting in slightly different anisotropic “content” in the simulated voltages. Here, we use the concept of “content” and consider the anisotropy as resulting in addition of a small deviation ( $\Delta \mathbf{d}_a$ ) to the measurements,  $\mathbf{d}_i$ , that would result from a purely isotropic model:  $\mathbf{d} = \mathbf{d}_i + \Delta \mathbf{d}_a$ .

This analysis suggests that the origin of these image errors is the fixed geometry of the FEM used in the image reconstruction. The Jacobian (sensitivity) matrix based on the fixed FEM will not have a range which includes the anisotropic “content”,  $\Delta \mathbf{d}_a$ . Such deviations will thus be associated with singular values of the Jacobian which are zero (or very small, depending on numerical error). During image reconstruction, these deviations thus cannot be explained by an inverse model parametrized only for isotropic conductivity, and will then be reconstructed as artefacts, which are projected onto the reconstructed image.

Given this source of image errors, we propose a modification of the reconstruction process to compensate for the anisotropic “content”. The key motivation is to allow the image reconstruction algorithm to vary the FEM geometry to “explain” the measurements. The reconstruction problem is formulated in terms of a regularized inverse, using an augmented Jacobian, sensitive to both conductivity and the position of FEM nodes. Image reconstruction then seeks to calculate both the element conductivities and the node positions which best conform to the data and prior model. For difference EIT, we consider EIT difference measurements,  $\mathbf{d} = F(\Delta \boldsymbol{\sigma})$ , originating

from isotropic conductivity changes  $\Delta\boldsymbol{\sigma}$  and augment the FEM model,  $F(\Delta\boldsymbol{\sigma}, \Delta\mathbf{r})$ , to consider the conductivity distribution,  $\Delta\boldsymbol{\sigma}$ , and the node positions,  $\Delta\mathbf{r}$ . Based on this model, we calculate a conductivity Jacobian,  $\mathbf{J}_c$  (the sensitivity of measurements to conductivity changes); and a movement Jacobian,  $\mathbf{J}_m$  (the sensitivity of measurements to node position movements),

$$[\mathbf{J}_c]_{ij} = \frac{\partial F_i(\Delta\boldsymbol{\sigma}, \Delta\mathbf{r})}{\partial [\Delta\boldsymbol{\sigma}]_j}, \text{ and} \quad (9)$$

$$[\mathbf{J}_m]_{ij} = \frac{\partial F_i(\Delta\boldsymbol{\sigma}, \Delta\mathbf{r})}{\partial [\Delta\mathbf{r}]_j}. \quad (10)$$

This approach follows the electrode movement analysis of Soleimani *et al* (2006) but the formulation is modified to include movement of all internal FEM nodes. Calculation of  $\mathbf{J}_c$  is performed normally, using the adjoint field (Vauhkonen *et al* 1999), while  $\mathbf{J}_m$  is calculated using the formulation of Gómez-Laberge and Adler (2008).

The standard linear solution,  $\hat{\mathbf{m}}$ , to (1) is

$$\hat{\mathbf{m}} = (\mathbf{J}^T \boldsymbol{\Sigma}_n^{-1} \mathbf{J} + \boldsymbol{\Sigma}_d^{-1})^{-1} \mathbf{J} \boldsymbol{\Sigma}_n^{-1} \mathbf{d} = \boldsymbol{\Sigma}_d \mathbf{J}^T (\mathbf{J} \boldsymbol{\Sigma}_d \mathbf{J}^T + \boldsymbol{\Sigma}_n)^{-1} \mathbf{d}, \quad (11)$$

assuming  $\mathbf{m}_0 = 0$ , as normally done for difference EIT.

Normally, the parameter vector,  $\hat{\mathbf{m}}$ , represents only the conductivity change,  $\Delta\boldsymbol{\sigma}$ . Instead, we represent our scheme using the conductivity change and vertex movement as parameters:  $\hat{\mathbf{m}} = [\Delta\boldsymbol{\sigma}^T | \Delta\mathbf{r}^T]^T$  and  $\mathbf{J} = [\mathbf{J}_c | \mathbf{J}_m]$ . In this case, the prior  $\boldsymbol{\Sigma}_d$  may be decomposed into

$$\boldsymbol{\Sigma}_d = \begin{bmatrix} \boldsymbol{\Sigma}_c & 0 \\ 0 & \boldsymbol{\Sigma}_m \end{bmatrix} \quad (12)$$

representing conductivity change,  $\boldsymbol{\Sigma}_c$ , and movement,  $\boldsymbol{\Sigma}_m$ , parts with no correlation assumed between these parameters (following Soleimani *et al* 2006), yielding:

$$\hat{\mathbf{m}} = \begin{bmatrix} \boldsymbol{\Sigma}_c \mathbf{J}_c^T \\ \boldsymbol{\Sigma}_m \mathbf{J}_m^T \end{bmatrix} (\mathbf{J}_c \boldsymbol{\Sigma}_c \mathbf{J}_c^T + \mathbf{J}_m \boldsymbol{\Sigma}_m \mathbf{J}_m^T + \boldsymbol{\Sigma}_n)^{-1} \mathbf{d} \quad (13)$$

Since we are only interested in displaying the reconstructed conductivity change,  $\Delta\hat{\boldsymbol{\sigma}}$ , only this fraction of (13) is used. Thus, standard and proposed reconstruction formulations differ only by the term  $\mathbf{J}_m \boldsymbol{\Sigma}_m \mathbf{J}_m^T$ :

$$\Delta\hat{\boldsymbol{\sigma}} = \begin{cases} \boldsymbol{\Sigma}_c \mathbf{J}_c^T (\mathbf{J}_c \boldsymbol{\Sigma}_c \mathbf{J}_c^T + \boldsymbol{\Sigma}_n)^{-1} \mathbf{d} & \text{standard} \\ \boldsymbol{\Sigma}_c \mathbf{J}_c^T (\mathbf{J}_c \boldsymbol{\Sigma}_c \mathbf{J}_c^T + \boldsymbol{\Sigma}_n + \mathbf{J}_m \boldsymbol{\Sigma}_m \mathbf{J}_m^T)^{-1} \mathbf{d} & \text{proposed} \end{cases} \quad (14)$$

The standard and proposed image reconstruction approaches (14) were implemented for the simulated data of figure 1, and are shown in figure 6. The proposed approach (bottom row) shows a significant reduction in image artefacts, but roughly the same resolution of the conductivity target.  $\boldsymbol{\Sigma}_m$  was chosen as the scaled identity matrix with an amplitude such that the noise figure (Adler and Guardo 1996a) reduced from 1.0 (standard) to 0.8 (proposed).

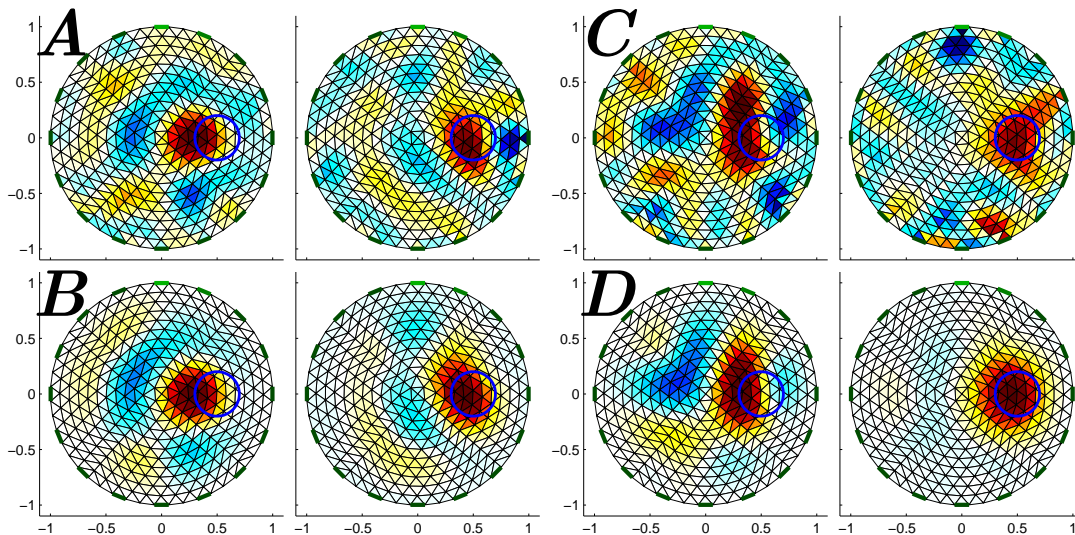


**Figure 6.** Reconstructed difference images calculated as in figure 1 for changes in FEM geometry. In each labelled image pair: *Left*: Coarse Mesh, *Right*: Fine Mesh. The target position is indicated by the blue circle. *A,B*: Data from 2D FEM; and *C,D*: Data from 3D FEM. *A,C*: Standard approach, and *B,D*: Proposed approach.

## 5. Discussion

This paper considers one limitation of finite element models for EIT image reconstruction. We propose the hypothesis that image reconstruction artefacts which occur due to changes in FEM geometry, as a result of projections of the element conductivity tensors onto the FEM system matrix. During image reconstruction, such anisotropic contributions cannot be represented in an isotropic model and are reconstructed as artefacts. The effect is proportional to the relative FEM geometry change,  $d/s$ , where  $d$  is the FEM node movement and  $s$  is the size of the element. This suggests that such anisotropic effects will continue to play an important role, even if very small FEM elements are used.

In order to compensate for this effect, we propose an augmented formulation of the EIT inverse problem and the inclusion of a FEM node movement term into the inverse term in (14), yielding  $(\mathbf{J}_c \boldsymbol{\Sigma}_c \mathbf{J}_c^T + \mathbf{J}_m \boldsymbol{\Sigma}_m \mathbf{J}_m^T + \boldsymbol{\Sigma}_n)^{-1}$ . Noting that the movement term is added to the “raw” instrument noise term  $\boldsymbol{\Sigma}_n$ , we may interpret  $\mathbf{J}_m \boldsymbol{\Sigma}_m \mathbf{J}_m^T$  as the correlated noise due to the structure of the FEM.

Several papers have considered related problems. Kohn and McKenney (1990) implemented a variational method, and proposed stabilising the inverse problem by allowing limited anisotropic conductivity. Kolehmainen *et al* (2007) develop an inverse solution in which they reconstruct an anisotropic conductivity and use that value to model a matching approximate isotropic conductivity. Tarvainen *et al* (2010) show that Bayesian reconstruction which considers both the first and second order statistics of model errors results in improved reconstructions in diffuse optical tomography. These errors were estimated from a distribution of coarse approximations to a fine FEM using

the approach of Kolehmainen *et al* (2009). Interestingly, (14) is equivalent to that proposed by Nissinen *et al* (2010) at the same conference in which we presented an early version of this work. This paper showed how addition of the FEM geometry term dramatically improves absolute image reconstructions in cases where the model geometry differs from the original measured one. While we arrive at the same expression as Nissinen *et al*, we approach the problem from a different perspective, and explain the importance of the contribution largely in terms of the contribution of anisotropic effects.

Our study has several limitations. We are guided by the hypothesis that these FEM errors are a result of anisotropic effects. While numerical evidence supports this interpretation, we do not prove this is the main (or only) effect. This study considers only first order FEM elements. Such elements suffer several limitations for EIT. Specifically, the formulation of such a FEM model requires voltage continuity across elements, but only fit current in an average (or weak) sense (Silvester and Ferrari 1990). This means that the voltages, but not the voltage gradients on elements, are guaranteed to converge pointwise with decreasing element size. However, EIT reconstruction depends on an accurate model of the sensitivity (Jacobian), which, in turn, depends on estimates of FEM gradients. We thus recommend that this analysis be conducted for higher order FEM elements to understand the importance of FEM geometry effects in these systems. Another limitation is that we only consider linear difference imaging, and reconstruct images comparing FEM solutions for two different meshes; while an absolute image solution would only involve one forward and one inverse solution FEM. For absolute imaging, it is also necessary to consider the interaction between errors due to the FEM and those due to limitations of the linear approximation.

In summary, these results help explain the strange effect that EIT simulations from adapted target meshes often show large artefacts, and also the effect that simulations of electrode movement show much larger effects than are observed in measured data. Additionally, these results suggest that EIT image reconstruction should allow for anisotropic behaviour in the measured signals. Thus, this work calls for consideration of FE models and the assumption of isotropic conductivity in EIT.

## 6. References

- Abascal JPJ, Arridge SR, Atkinson D, Horesh R, Fabrizi L, Horesh L, Bayford RH, Holder DS 2008 Use of anisotropic modelling in electrical impedance tomography; Description of method and preliminary assessment of utility in imaging brain function in the adult human head *NeuroImage* 43:258–268
- Abascal JPJ, Lionheart WRB, Arridge SR, Schweiger M, Atkinson D, Holder DS 2011 Electrical impedance tomography in anisotropic media with known eigenvectors In Press: *Inverse Problems*
- Adler A and Guardo R 1996a Electrical impedance tomography: regularized imaging and contrast detection *IEEE T Med. Imaging* 15 170-179
- Adler A, Guardo R and Berthiaume Y 1996b Impedance imaging of lung ventilation: Do we need to account for chest expansion? *IEEE T Biomed. Eng.* 43(4) 414-20
- Adler A Borsic A Polydorides N Lionheart W R B 2008 Simple FEMs aren't as good as we thought: experiences developing EIDORS v3.3 *Proc. Conf. EIT*, Hannover, NH, USA

- Barber D C and Brown B H 1988 Errors in reconstruction of resistivity images using a linear reconstruction technique *Clin. Phys. Physiol. Meas.* 9(suppl. A) 101–4
- Breckon WR, Pidcock MK, 1988 Ill-Posedness and Non-Linearity in Electrical-Impedance Tomography, *Information Processing in Medical Imaging*, Ed de Graaf and Viergever, pp. 235–244, Plenum
- Cheney M, Isaacson D, Newell J C, Simske S and Goble J C 1990 NOSER: an algorithm for solving the inverse conductivity problem *Int J Imaging Syst Technol* 2 66–75
- Gagnon H, Cousineau M, Adler A, Hartinger A 2010 A resistive mesh phantom for assessing the performance of EIT systems *IEEE T Biomed. Eng.* 57:2257–2266, 2010.
- Gómez-Laberge C Adler A 2008 Direct EIT Jacobian calculations for conductivity change and electrode movement *Physiol Meas* 29 S89–S99
- Herwanger JV, Pain CC, Binley A, De Oliveira CRE, Worthington MH (2004), Anisotropic resistivity tomography. *Geophysical Journal International* 158 409–425.
- Holder DS, ed. 2005 *Electrical Impedance Tomography*. Institute of Physics Publishing, Bristol and Philadelphia.
- Kolehmainen V, Lassas M and Ola P 2007 The inverse conductivity problem with an imperfectly known boundary in three dimensions *SIAM J Applied Math* 67 1440–1452
- Kolehmainen V, Schweiger M, Nissilä I, Tarvainen T, Arridge SR, Kaipio JP, 2009 “Approximation errors and model reduction in three-dimensional diffuse optical tomography, *J. Opt. Soc. Am. A* 26, 22572268,
- Murai T, Kagawa Y 1985 Electrical impedance computed tomography based on finite element model *IEEE T Biomed Eng* 32:177-184
- Nissinen A, Kolehmainen, V, Kaipio, JP 2010 Compensation of errors due to incorrect model geometry in electrical impedance tomography *Proc. Conf. ICEBI & EIT*, Gainesville, FL, USA, 4–8 Apr
- Schöberl J 1997 NETGEN: An advancing front 2D/3D-mesh generator based on abstract rules *Computing and Visualization in Science* 1 41–52
- Seagar A D Bates R H T 1985 Full-wave computed tomography. Part 4: Low-frequency electric current *CT IEE Proceedings A* 132: 455–466
- Soleimani M, Gómez-Laberge C and Adler A 2006 Imaging of conductivity changes and electrode movement in EIT *Physiol Meas* 27 S103–S13
- Silvester PP and Ferrari RL, 1990, *Finite Elements for Electrical Engineers*, Cambridge University Press
- Tarvainen T, Kolehmainen V, Kaipio JP, Arridge SR 2010, “Corrections to linear methods for diffuse optical tomography using approximation error modelling”, *Biomedical Optics Express* 1(1) 209-222
- Vauhkonen P Vauhkonen M Savolainen T and Kaipio JP 1999 Three-dimensional electrical impedance tomography based on the complete electrode model. *IEEE T Biomed Eng* 46 1150–1160
- Yorkey T J, Webster J G and Tompkins W J 1987 Comparing reconstruction algorithms for electrical impedance tomography *IEEE Trans. Biomed. Eng* 34 843–52
- Yang F Patterson R 2007 The contribution of the lungs to thoracic impedance measurements: a simulation study based on a high resolution finite difference model *Physiol. Meas.* 28 S153–S163